Equivalent Circuit Models for Computer Aided Design of Microstrip Rectangular Structures

Franco Giannini, Giancarlo Bartolucci, and Marina Ruggieri, *Member, IEEE*

Abstract—**A new modeling of microstrip rectangular structures in terms of equivalent circuits is here illustrated to overcome many of the drawbacks and limitations of previously proposed approaches and the poor accuracy still introduced by most of the presently available models. Through a successful electromagnetic approach, a lumped element modeling for interacting and non-interacting step discontinuities have been created and tested. An alternative modeling is also proposed to account for shunt connected double and single stubs in cross and tee junction with the main line respectively. The different models have also been tested on the same structure to demonstrate their congruency.**

I. Introduction

THE WIDESPREAD use of monolithic microwave integrated circuits (MMIC's) and the growing demand for high working frequencies underline a continuous need for accurate and dependable predictions of the behavior of microstrip *passive* components.

With this respect, the deep effort paid until now to the development of microwave circuit design techniques are now being focused on the assessment of electromagnetic approaches to solve circuital issues.

On the other hand, commercial CAD software has been developed mostly for the design of hybrid microwave integrated circuits, where a moderate precision can be accepted. The latter is allowed both by the modest accuracy in active device characterization through data-sheets and by the unpredictable but effective final tuning on the manufactured circuit.

Only recently the commercial CAD software has started to move toward fully monolithic-oriented solutions. The turning point for a complete "conversion" is mostly represented by an effective modeling of both active and passive components. Many new ideas and developments are still expected from this point of view.

Paying attention to the models of passive components generally included in commercial CAD software, it is worth noting that they are mainly based on a quasi-static approximation that limits their validity to quite low frequencies. This is, for instance, the case of the microstrip double step discontinuity, which is largely widespread in integrated circuits for impedance transitions, filtering, broadband matching, etc.

In recent years, deep efforts have been devoted to the development of accurate and effective characterization techniques for this kind of discontinuity [1]–[4].

One of those approaches has produced closed formulas [5], [6], which, however, solve formally but not substantially the characterization task, mostly because of their complicated frequency dependence.

An alternative approach has consisted of an equivalent representation through almost fully frequency-independent elements [7]. The achievable model, however, is quite complicated and unfriendly to handle, resulting in the inability to separate properly the "main" and the "parasitic" effects of the actual structure.

The present contribution is intended to derive and test some new equivalent circuits for rectangular microstrip structures through a modelling that is tightly related to their physical behavior, so allowing a better understanding of the e.m. phenomena involved.

The circuits, which are derived from an effective planar dynamic approach and are developed according to the technique pioneered by [9], provide frequency-independent equivalent elements, broadband validity and CAD-oriented implementation.

In particular, the proposed equivalent circuits treat the rectangular microstrip structure as either closely-spaced (interacting) and apart (non-interacting) microstrip step-discontinuities [8], or as double [10] or as single open stub in shunt connection to the main line.

Moreover, although the use of each one would be advisable where specific geometric ratios are met by the structure, the derivation of the different equivalent circuits from the *same* electromagnetic approach assures an intrinsic congruency in the provided results whatever the structure's geometrical parameters. This particular feature, among the others, has been checked and the corresponding results are presented and commented.

II. Theoretical Characterization

A theoretical characterization based on the electromagnetic behavior of the structures seems to be the best approach to obtain the desired accuracy in the simulation of passive networks.

In recent years, in fact, several models have been proposed [1], [2] and CAD programs have been presented or

Manuscript received April 15, 1991; revised August 13, 1991.

F. Giannini and G. Bartolucci are with the University of Rome "Tor Vergata," Department of Electronics Engineering, Via Orazio Raimondo, 00173 Rome, Italy.

M. Ruggieri is with the University of L'Aquila, Department of Electrical Engineering 67040 Poggio di Roio, L'Aquila, Italy.

IEEE Log Number 9104778.

announced, all based on an electromagnetic approach. Although often very rigorous, those methods seem often to be quite complicated to use and implement.

On the contrary, the development of lumped element equivalent circuits based on the electromagnetic approach represent a proper merging of the required accuracy with the availability of friendly tools, effectively usable in practical circuit design and optimization and very easy to relate to the physical geometry.

The new modeling, which fully meets those requirements, derives from the characterization of the rectangular microstrip structure in terms of a resonant mode field expansion technique, described in [7], [11], [12].

According to this theory, the analysis of a two port planar microwave network like the one depicted in Fig. 1 for a symmetrical case, can be performed evaluating, in the rectangular domain, the orthonormalized set of eigenfunctions of the bidimensional Helmholtz equation with homogeneous Neumann boundary conditions.

Under the hypotheses of negligible losses, evanescent higher order modes on the connecting lines and line widths much smaller with respect to the structure dimensions, the following equation can be written for the impedance matrix $[Z]$ of the network:

$$[Z] = \sum_{m=0}^{\infty} \sum_{n=0}^{\infty} [Z_{mn}] \tag{1}$$

where

$$[Z_{mn}] = \frac{j\omega\mu h}{K_{mn}^2 - \omega^2 \mu \epsilon_{m,n}} \begin{bmatrix} P_{mn1}^2 & P_{mn1} P_{mn2} \\ P_{mn1} P_{mn2} & P_{mn2}^2 \end{bmatrix} \tag{2}$$

with

$$P_{mnj} = \frac{1}{w_{j\text{eff}}} \int_{s_j} \Psi_{mn}\, ds \qquad j = 1, 2 \tag{3}$$

and s_j the portion on the planar structure contour corresponding to the j-port; $\Psi_{m,n}$ and $K_{m,n}^2$ the eigenfunction and the eigenvalue of the (m, n)-th mode; h the substrate thickness; $w_{j\text{eff}}$ the effective width of the jth line. Moreover $\epsilon_{m,n}$ is the effective permittivity of the (m, n)th mode evaluated after [13].

Inserting (2) and (3) in (1) it is possible to obtain the following specialized equations for the Z-parameters of a symmetrical structure (see Fig. 1):

$$Z_{11} = Z_{22} = \frac{j\omega\mu h}{bl} \sum_{m=0}^{\infty} \sum_{n=0}^{\infty} \frac{\delta_m\, \delta_n g_n^2}{K_{m,2n}^2 - \omega^2 \mu \epsilon_{m,2n}} \tag{4}$$

$$Z_{12} = Z_{21} = \frac{j\omega\mu h}{bl} \sum_{m=0}^{\infty} \sum_{n=0}^{\infty} \frac{\delta_m\, \delta_n g_n^2 (-1)^m}{K_{m,2n}^2 - \omega^2 \mu \epsilon_{m,2n}} \tag{5}$$

where

$$K_{m,2n}^2 = \pi^2 [(m/l)^2 + (2n/b)^2] \tag{6}$$

$$\delta_m = \begin{cases} 1 & m = 0 \\ 2 & m \neq 0 \end{cases} \tag{6'}$$

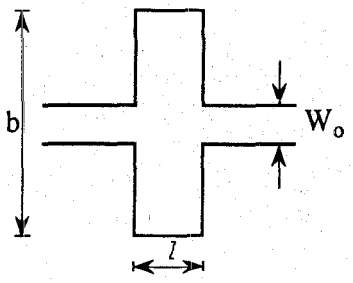

Fig. 1. A microstrip rectangular structure (symmetrical case).

$$g_n = \sin\left(\frac{n\pi w_0}{b}\right) \Big/ \left(\frac{n\pi w_0}{b}\right) \tag{6''}$$

with b, l and w_0 effective dimensions of the rectangular microstrip structure, evaluated after [13].

A. The Double-Step Discontinuity

The expressions (4), (5) for the $[Z]$ matrix elements of a symmetrical rectangular microstrip can be properly rearranged as [8]:

$$Z_{11} = Z_{22} = \frac{j\omega\mu h}{bl} \left[\sum_{m=0}^{\infty} \frac{\delta_m}{K_{m,0}^2 - \omega^2 \mu \epsilon_{m,0}} + \sum_{n=1}^{\infty} \sum_{m=0}^{\infty} \frac{2\delta_m g_n^2}{K_{m,2n}^2 - \omega^2 \mu \epsilon_{m,2n}} \right] = Z_{11l} + Z_A \tag{7}$$

$$Z_{12} = Z_{21} = \frac{j\omega\mu h}{bl} \left[\sum_{m=0}^{\infty} \frac{\delta_m (-1)^m}{K_{m,0}^2 - \omega^2 \mu \epsilon_{m,0}} + \sum_{n=1}^{\infty} \sum_{m=0}^{\infty} \frac{2\delta_m g_n^2 (-1)^m}{K_{m,2n}^2 - \omega^2 \mu \epsilon_{m,2n}} \right] = Z_{12l} + Z_B \tag{8}$$

where

$$Z_A = \frac{j\omega\mu h}{bl} \left[\sum_{n=1}^{\infty} \sum_{m=0}^{\infty} \frac{2\delta_{2m} g_n^2}{K_{2m,2n}^2 - \omega^2 \mu \epsilon_{2m,2n}} + \sum_{n=1}^{\infty} \sum_{m=0}^{\infty} \frac{2\delta_{2m+1} g_n^2}{K_{2m+1,2n}^2 - \omega^2 \mu \epsilon_{2m+1,2n}} \right] = Z_{\text{ev}} + Z_{\text{od}} \tag{9}$$

$$Z_B = \frac{j\omega\mu h}{bl} \left[\sum_{n=1}^{\infty} \sum_{m=0}^{\infty} \frac{2\delta_{2m} g_n^2}{K_{2m,2n}^2 - \omega^2 \mu \epsilon_{2m,2n}} - \sum_{n=1}^{\infty} \sum_{m=0}^{\infty} \frac{2\delta_{2m+1} g_n^2}{K_{2m+1,2n}^2 - \omega^2 \mu \epsilon_{2m+1,2n}} \right] = Z_{\text{ev}} - Z_{\text{od}} \tag{10}$$

with Z_{ev} and Z_{od}, summations of all the terms having an even and odd "m" index, respectively.

Finally, from (7)–(10):

$$[Z] = \begin{bmatrix} Z_{11l} & Z_{12l} \\ Z_{21l} & Z_{22l} \end{bmatrix} + \begin{bmatrix} Z_A & Z_B \\ Z_B & Z_A \end{bmatrix} = [Z]_l + [Z']. \tag{11}$$

The corresponding $[Z]$ matrix can be so considered as the sum of two $[Z]$ matrices, one, the $[Z]_l$ matrix, corre-

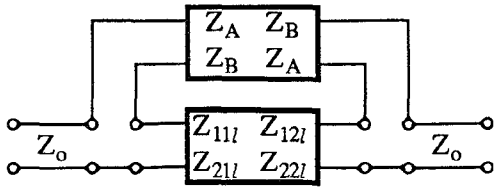

Fig. 2. Double step discontinuity represented in terms of two-port networks.

sponding to the two-port representation for a microstrip line of effective length l and width b, and the other one, the $[Z']$ matrix, corresponding to a two-port network in series connection to the first one (Fig. 2), that can be assumed to represent the effect of the two interacting step-discontinuities.

More precisely, the interaction between the two step discontinuities has been taken into account through the Z_B term, which generalizes a previously proposed approach to a similar problem, corresponding to the introduction of some "parasitic elements" [14].

Fig. 3 shows the behavior of Z_B when widening the rectangular microstrip dimension (l) for different transversal size (b) and fixed substrate parameters. From those plots it may be inferred how the simple case of non-interacting discontinuities is represented when Z_B approaches zero, that is when Z_{ev} approaches Z_{od}.

B. An Alternative Approach

When the structure in Fig. 1 shows a stronger development in the transversal direction ($b >> l$) it can be more effectively described as two open stubs in shunt connection to a main line rather than as two (closely-spaced) cascaded step-discontinuities. In this case an alternative approach can be more effectively followed for its characterization.

An improvement in the correspondence between theoretical model and physical geometry and an overall lower circuit complexity can be so achieved.

The different model can be derived by a different rearranging of the $[Z]$ matrix element equations, able to point out the contributions along the transversal direction (b) instead of those along the longitudinal one (l) as in (7)–(11).

The alternative approach has been also applied to the structure in Fig. 4, which has been modeled as a single open stub in shunt connection.

C. Double-Stub in Cross Connection

The Z_{ij} expressions, rearranged for the structure in Fig. 1, provide [10]:

$$Z_{11} = Z_{22} = \frac{j\omega\mu h}{bl}\left[\sum_{n=0}^{\infty}\frac{\delta_{2n}g_{2n}^2}{K_{0,2n}^2-\omega^2\mu\epsilon_{0,2n}} + \sum_{n=0}^{\infty}\sum_{m=1}^{\infty}\frac{2\delta_{2n}g_{2n}^2}{K_{m,2n}^2-\omega^2\mu\epsilon_{m,2n}}\right] = Z_S + Z_\alpha - Z_\gamma \tag{12}$$

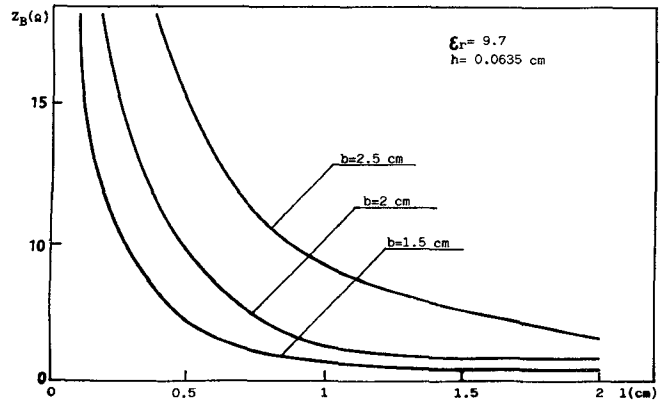

Fig. 3. Interaction degree between the two step discontinuities versus structure geometrical dimensions (b, l).

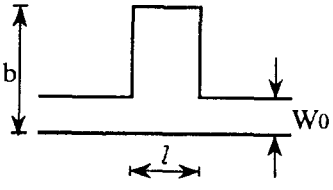

Fig. 4. Microstrip rectangular structure (single stub in tee connection).

$$Z_{12} = Z_{21} = \frac{j\omega\mu h}{bl}\left[\sum_{n=0}^{\infty}\frac{\delta_{2n}g_{2n}^2}{K_{0,2n}^2-\omega^2\mu\epsilon_{0,2n}} + \sum_{n=0}^{\infty}\sum_{m=1}^{\infty}(-1)^m\frac{2\delta_{2n}g_{2n}^2}{K_{m,2n}^2-\omega^2\mu\epsilon_{m,2n}}\right] = Z_S + Z_\beta - Z_\gamma \tag{13}$$

where $K_{m,2n}$, δ_n and g_n are the same as in (6), (6)′, (6)″ and

$$Z_S = \frac{j\omega\mu h}{bl}\sum_{n=0}^{\infty}\frac{\delta_{2n}}{K_{0,2n}^2-\omega^2\mu\epsilon_{0,2n}} = -j\frac{Z_{os}}{2}\operatorname{cotg}\frac{\omega b}{2c} \quad \text{with } Z_{os} = \sqrt{\mu/\epsilon}\,(h/l) \tag{14}$$

$$Z_\alpha = \frac{j\omega\mu h}{bl}\left[\sum_{m=1}^{\infty}\sum_{n=0}^{\infty}\frac{2\delta_{2n}g_{2n}^2}{K_{2m,2n}^2-\omega^2\mu\epsilon_{2m,2n}} + \sum_{m=1}^{\infty}\sum_{n=0}^{\infty}\frac{2\delta_{2n}g_{2n}^2}{K_{2m-1,2n}^2-\omega^2\mu\epsilon_{2m-1,2n}}\right] = Z_{\overline{ev}} + Z_{\overline{od}} \tag{15}$$

$$Z_\beta = \frac{j\omega\mu h}{bl}\left[\sum_{m=1}^{\infty}\sum_{n=0}^{\infty}\frac{2\delta_{2n}g_{2n}^2}{K_{2m,2n}^2-\omega^2\mu\epsilon_{2m,2n}} - \sum_{m=1}^{\infty}\sum_{n=0}^{\infty}\frac{2\delta_{2n}g_{2n}^2}{K_{2m-1,2n}^2-\omega^2\mu\epsilon_{2m-1,2n}}\right] = Z_{\overline{ev}} - Z_{\overline{od}} \tag{16}$$

$$Z_\gamma = \frac{j\omega\mu h}{bl}\sum_{n=0}^{\infty}\frac{(1-g_{2n}^2)\delta_{2n}}{K_{0,2n}^2-\omega^2\mu\epsilon_{0,2n}} = \frac{j\omega\mu h}{bl}\sum_{n=1}^{\infty}\frac{2(1-g_{2n}^2)}{K_{0,2n}^2-\omega^2\mu\epsilon_{0,2n}} \tag{17}$$

where all the entries have the previously depicted meanings.

The Z-parameters expressed through (12)–(17) are presented as sum of different contributions: $Z_{\overline{ev}}$ and $Z_{\overline{od}}$ are summations of all the terms in (15)–(16) having an even and odd "m" index, respectively; Z_γ takes into account the finite width of the structure feeding ports; Z_S is the input impedance of two shunt stubs having characteristic impedance Z_{os} (width W_{os}) and length $b/2$.

D. Single-Stub in Tee Connection

The characterization based on the "transversal direction" approach has been applied to the structure in Fig. 4, by rearrangement of the [Z] matrix element expressions removing the assumption of symmetrical structure geometry in the longitudinal direction.

The Z_{ij} expressions thus become

$$Z_{11} = Z_{22} = \frac{j\omega\mu h}{bl}\left[\sum_{n=0}^{\infty}\frac{\delta_n g_n^2}{K_{0,n}^2-\omega^2\mu\epsilon_{0,n}} + \sum_{n=0}^{\infty}\sum_{m=1}^{\infty}\frac{2\delta_n g_n^2}{K_{m,n}^2-\omega^2\mu\epsilon_{m,n}}\right] = Z_{\tilde{S}} + Z_{\tilde{\alpha}} - Z_{\tilde{\gamma}} \tag{18}$$

$$Z_{12} = Z_{21} = \frac{j\omega\mu h}{bl}\left[\sum_{n=0}^{\infty}\frac{\delta_n g_n^2}{K_{0,n}^2-\omega^2\mu\epsilon_{0,n}} + \sum_{n=0}^{\infty}\sum_{m=1}^{\infty}(-1)^m\frac{2\delta_n g_n^2}{K_{m,n}^2-\omega^2\mu\epsilon_{m,n}}\right] = Z_{\tilde{S}} + Z_{\tilde{\beta}} - Z_{\tilde{\gamma}} \tag{19}$$

where

$$K_{m,n}^2 = \pi^2[(m/l)^2 + (n/b)^2] \tag{20}$$

$$g_n = \sin\left(\frac{n\pi w_0}{2b}\right)\Big/\frac{n\pi w_0}{2b} \tag{20'}$$

δ_n is the same as in (6)′ and

$$Z_{\tilde{S}} = \frac{j\omega\mu h}{bl}\sum_{n=0}^{\infty}\frac{\delta_n}{K_{0,n}^2-\omega^2\mu\epsilon_{0,n}} = -jZ_{os}\operatorname{cotg}\frac{\omega b}{c} \tag{21}$$

with Z_{os} defined as in (14) and

$$Z_{\tilde{\alpha}} = \frac{j\omega\mu h}{bl}\left[\sum_{m=1}^{\infty}\sum_{n=0}^{\infty}\frac{2\delta_n g_n^2}{K_{2m,n}^2-\omega^2\mu\epsilon_{2m,n}} + \sum_{m=1}^{\infty}\sum_{n=0}^{\infty}\frac{2\delta_n g_n^2}{K_{2m-1n}^2-\omega^2\mu\epsilon_{2m-1,n}}\right] = Z_{\text{ev}} + Z_{\text{od}} \tag{22}$$

$$Z_{\tilde{\beta}} = \frac{j\omega\mu h}{bl}\left[\sum_{m=1}^{\infty}\sum_{n=0}^{\infty}\frac{2\delta_n g_n^2}{K_{2m,n}^2-\omega^2\mu\epsilon_{2m,n}} - \sum_{m=1}^{\infty}\sum_{n=0}^{\infty}\frac{2\delta_n g_n^2}{K_{2m-1,n}^2-\omega^2\mu\epsilon_{2m-1,n}}\right] = Z_{\text{ev}} - Z_{\text{od}} \tag{23}$$

$$Z_{\tilde{\gamma}} = \frac{j\omega\mu h}{bl}\sum_{n=0}^{\infty}\frac{(1-g_n^2)\delta_n}{K_{0,n}^2-\omega^2\mu\epsilon_{0,n}} = \frac{j\omega\mu h}{bl}\sum_{n=1}^{\infty}\frac{2(1-g_n^2)}{K_{0,n}^2-\omega^2\mu\epsilon_{0,n}} \tag{24}$$

being all the parameters as previously defined.

$Z_{\tilde{S}}$ represents the input impedance of a single shunt stub having characteristic impedance Z_{os} and length b, in shunt connection with the main line of width w_0.

III. The Equivalent Lumped Circuit

The formulation (7)–(11) can be translated in an equivalent circuit of the double step discontinuity, which shows several interesting and effective features:

1) It is derived from a *planar* approach that has been demonstrated to be effective in many applications.
2) It is based on a *dynamic* approach, so to fully describe the frequency behavior of the discontinuities, including their interaction due to the excitation of higher order modes, thus overcoming the limits of the quasi-static approximation.
3) The values of the equivalent components are practically *not* frequency-dependent, with the exception for the obvious but very moderate dispersion effect, thus avoiding the limited usefulness of already proposed frequency dependent equivalent elements.
4) The frequency bandwidth of validity is much broader with respect to similar previously proposed models and it has the intrinsic potential for further broadening, by adding more lumped element cells to the model.
5) It is easy to be implemented in the presently available commercial packages.

Starting from the formulation (7)–(11), the overall two-port network in Fig. 2 can be translated into the equivalent circuit reported in Fig. 5(a), where Z_{ev} and Z_{od} (as detailed in Fig. 5(b)) represent the series of parallel resonant LC cells and of an inductance, the latter accounting for the residual electromagnetic effects. The number of LC cells depends on the frequency range of operation and the specific structure geometry.

The elements of the resonant cells can be derived from the Z_{ev} and Z_{od} expressions contained in (9) and (10). The following form results:

$$Z_{\text{ev}} = \frac{j\omega\mu h}{bl}\sum_{n=1}^{\infty}\sum_{m=0}^{\infty}\frac{2\delta_{2m}g_n^2}{K_{2m,2n}^2-\omega^2\mu\epsilon_{2m,2n}} = j\omega\sum_{n=1}^{\infty}\sum_{m=0}^{\infty}\frac{L_{m,n}^{\text{ev}}}{1-\omega^2L_{m,n}^{\text{ev}}C_{m,n}^{\text{ev}}} \tag{25}$$

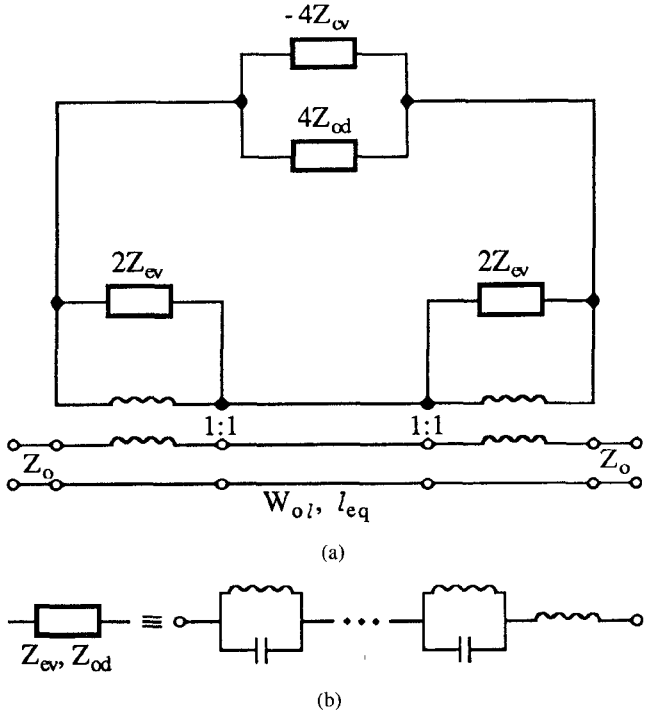

Fig. 5. (a) Equivalent circuit of the network in Fig. 2 (b) Detail of the Z_{ev} and Z_{od} blocks.

where

$$L^{ev}_{m,n} = \frac{\mu h}{bl}\frac{2\delta_{2m} g_n^2}{K^2_{2m,2n}} \tag{25}'$$

$$C^{ev}_{m,n} = \frac{bl}{h}\frac{\epsilon_{2m,2n}}{2\delta_{2m} g_n^2} \tag{25}''$$

and

$$Z_{od} = \frac{j\omega\mu h}{bl}\sum_{n=1}^{\infty}\sum_{m=0}^{\infty}\frac{4g_n^2}{K^2_{2m+1,2n} - \omega^2\mu\epsilon_{2m+1,2n}} = j\omega\sum_{n=1}^{\infty}\sum_{m=0}^{\infty}\frac{L^{od}_{m,n}}{1 - \omega^2 L^{od}_{m,n} C^{od}_{m,n}} \tag{26}$$

where

$$L^{od}_{m,n} = \frac{\mu h}{bl}\frac{4g_n^2}{K^2_{2m+1,2n}} \tag{26}'$$

$$C^{od}_{m,n} = \frac{bl}{h}\frac{\epsilon_{2m+1,2n}}{4g_n^2} \tag{26}''$$

Furthermore, the inductance in Fig. 5(b) consists of the sum of all residual contributions in (25) and (26) which are not directly taken into account in the model by *LC* cells.

The model is evaluated at the center frequency of the bandwidth where the structure behavior simulation or optimization is needed.

The complexity of the model, in terms of number of cells in the Z_{ev} and Z_{od} blocks, for a given structure is strictly dependent on its geometrical dimensions, the latter being related to the type and the finite number of modes that properly describe the structure. Normally, only modes having their resonant frequency as high as the upper limit of the frequency bandwidth under consideration have to be directly taken into account in terms of the corresponding *LC* cells.

As an example, the equivalent circuit is reported in Figs. 6 and 7 for two specific geometries, presenting the same transversal dimension $b = 1.5$ cm and different longitudinal ones ($l = 0.68$ cm and $l = 0.9$ cm respectively), assuming an alumina substrate ($\epsilon_r = 9.7$) 0.0635 cm thick. The breakdown of the two lumped circuits is summarized in Tables I and II respectively, detailing the composition of the Z_{ev} and Z_{od} blocks and the element values.

The lumped circuit of the $l = 0.68$ cm structure is evaluated at 7 GHz, which is about the midband frequency; an equivalent length $l_{eq} = 0.7$ cm ($W_{ol} = 1.5$ cm) has to be considered for the transmission line between the discontinuities.

In the case of the $l = 0.9$ structure, the lumped elements are evaluated at 5 GHz; the equivalent line length results to be $l_{eq} = 0.93$ cm ($W_{ol} = 1.5$ cm).

The alternative formulation (12)–(17) also leads to an equivalent circuit, presenting the discussed features and advantages. In particular the model displayed in Fig. 8 results.

As for the step discontinuity equivalent circuit, also in the present case the number of *LC* cells depends on the working frequency range and the structure geometry, while the inductance accounts for the residual electromagnetic effects.

The elements of the resonant cells can be derived from the $Z_{\overline{ev}}$ and $Z_{\overline{od}}$ expressions contained in (15)–(16), resulting in

$$Z_q = j\omega\sum_{m=1}^{\infty}\sum_{n=0}^{\infty}\frac{L^q_{m,n}}{1 - \omega^2 L^q_{m,n} C^q_{m,n}} \qquad q = \overline{ev},\ \overline{od},\ \gamma \tag{27}$$

where

$$L^q_{m,n} = \frac{\mu h}{bl}\frac{2\delta_{2n} g^2_{2n}}{K^2_{2m-r,2n}} \tag{28}'$$

$$C^q_{m,n} = \frac{bl}{h}\frac{\epsilon_{2m-r,2n}}{2\delta_{2n} g^2_{2n}} \tag{28}''$$

with

$$r = \begin{cases} 0 & q = \overline{ev} \\ 1 & q = \overline{od} \end{cases} \tag{29}$$

and

$$L^q_n = \frac{\mu h}{bl}\frac{2(1 - g^2_{2n})}{K^2_{0,2n}} \tag{30}$$

$$C^q_n = \frac{bl}{h}\frac{\epsilon_{0,2n}}{2(1 - g^2_{2n})} \tag{30}'$$

when $q = \gamma$.

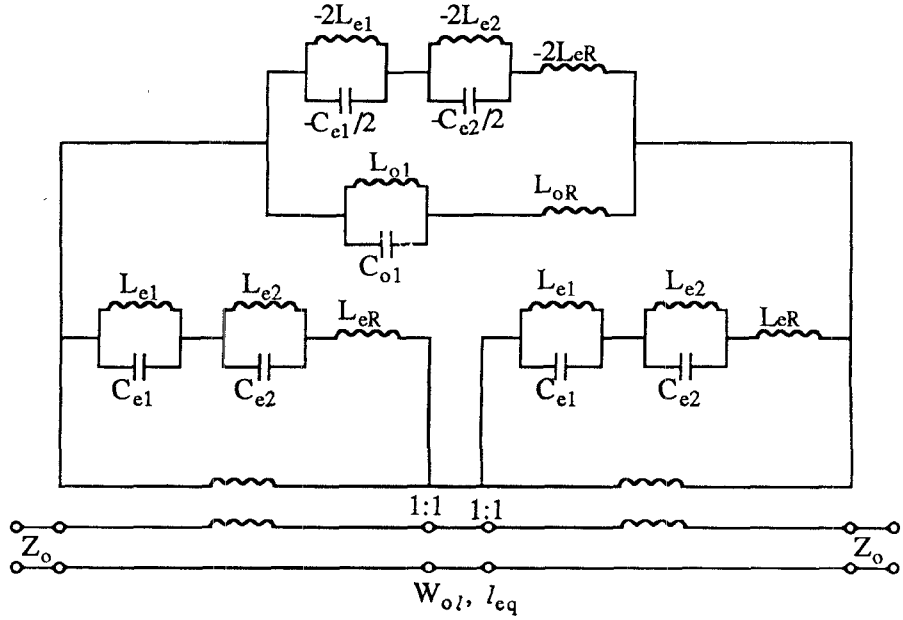

Fig. 6. Step discontinuity equivalent circuit for a rectangular microstrip structure with $b = 1.5$ cm and $l = 0.68$ cm.

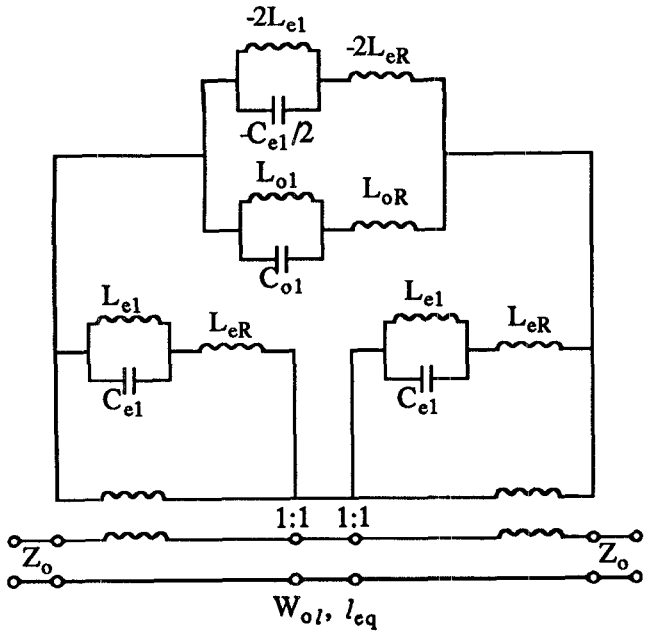

Fig. 7. Step discontinuity equivalent circuit for a rectangular microstrip structure with $b = 1.5$ cm and $l = 0.9$ cm.

TABLE I
BREAKDOWN OF THE EQUIVALENT CIRCUIT IN FIG. 6 FOR THE 1.5 × 0.68 cm STRUCTURE

	First Cell		Second Cell		Residual Inductance
	L_1(nH)	C_1 (pF)	L_2 (nH)	C_2 (pF)	L_R (nH)
$2Z_{ev}$	0.1374	4.0758	0.0386	4.2269	0.2567
$4Z_{od}$	0.3106	0.8708	—	—	0.4859

TABLE II
BREAKDOWN OF THE EQUIVALENT CIRCUIT IN FIG. 7 FOR THE 1.5 × 0.9 cm STRUCTURE

	First Cell		Residual Inductance
	L_1 (nH)	C_1 (pF)	L_R (nH)
$2Z_{ev}$	0.1284	4.9281	0.2917
$4Z_{od}$	0.3059	1.140	0.3298

The alternative lumped circuit is applied to two rectangular structures, differing in the transversal dimension, assuming a 0.0254 cm thick alumina substrate ($\epsilon_r = 9.9$). The two equivalent circuits are displayed in Fig. 9 for a $b = 0.785$ cm × $l = 0.051$ cm structure and in Fig. 10 for a $b = 0.353$ cm × $l = 0.051$ cm structure. In Tables III and IV the detailed breakdown of the circuits are reported respectively.

The lumped elements of the two circuits are evaluated at 16 GHz. An equivalent length $b_{eq}/2$ has to be considered for the stubs; in the present case, $b_{eq}/2 = 0.397$ cm ($W_{os} = 0.051$ cm) and $b_{eq}/2 = 0.185$ cm ($W_{os} = 0.051$ cm), respectively.

In Fig. 11 and Table V the equivalent circuit schematic and breakdown of the rectangular structure with $b = 1.5$ cm and $l = 0.68$ cm (0.0635 cm thick alumina substrate) already considered in testing the step discontinuity model are reported. The circuit elements are evaluated at 5 GHz and $b_{eq}/2 = 0.772$ cm has been considered ($W_{os} = 0.68$ cm).

The formulation (18)–(24) for the rectangular structure in Fig. 4, treated as single stub in shunt connection, leads to the equivalent model displayed in Fig. 12 and expressions for the cell elements that are identical to those derived for the cross-junction formulation (27)–(30)′ when replacing the "$2n$" index with "n".

The lumped circuit is utilized for two different structures assuming a 0.0254 cm thick alumina substrate ($\epsilon_r = 9.9$). The two circuits are depicted in Fig. 13 for a $b =$

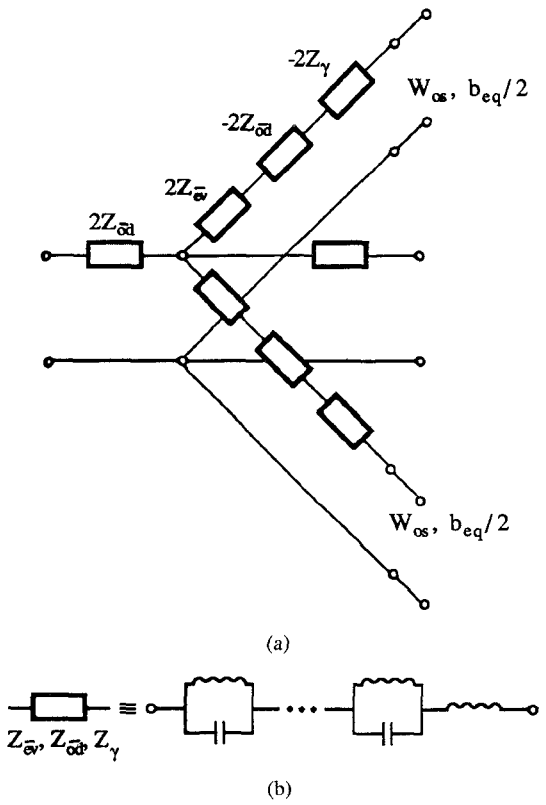

Fig. 8. (a) Cross junction based equivalent circuit of the microstrip rectangular structure. (b) Detail of the $Z_{\bar{ev}}$, $Z_{\bar{od}}$, Z_{γ}, blocks.

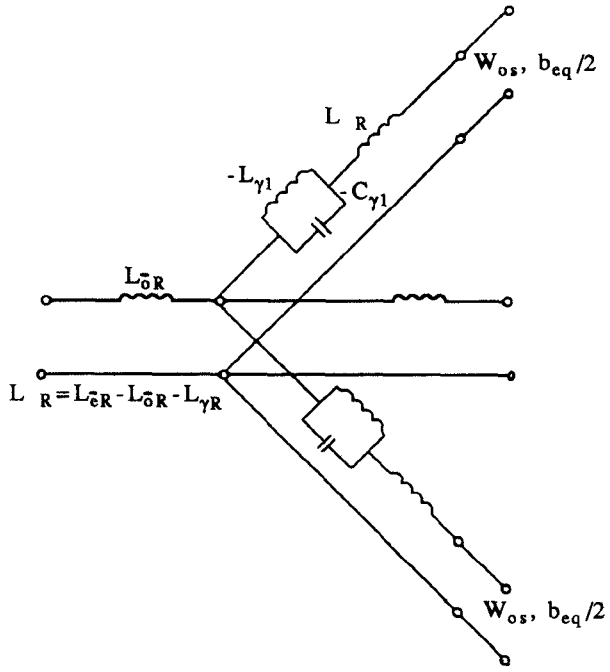

Fig. 9. Cross junction based equivalent circuit for a rectangular microstrip structure with b = 0.785 cm and l = 0.051 cm.

$0.176 \times l = 0.051$ cm structure and in Fig. 14 for a $b = 0.226$ cm $\times$ $l = 0.051$ cm structure. In Tables VI and VII the detailed breakdown of the circuits are reported respectively.

The lumped elements of both circuits are evaluated at

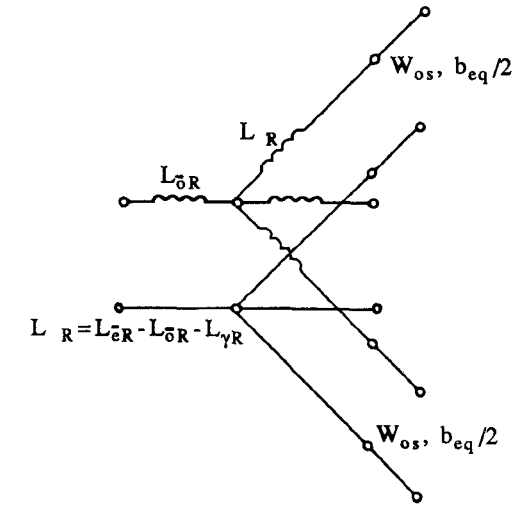

Fig. 10. Cross junction based equivalent circuit for a rectangular microstrip structure with b = 0.353 cm and l = 0.051 cm.

TABLE III
BREAKDOWN OF THE EQUIVALENT CIRCUIT IN FIG. 9 FOR THE 0.785 × 0.051 cm STRUCTURE

	First Cell		Residual Inductance
	L_1 (nH)	C_1 (pF)	L_R (nH)
$2Z_{\bar{ev}}$	—	—	0.0357
$2Z_{\bar{od}}$	—	—	0.1080
$2Z_{\gamma}$	0.0066	19.3602	0.0794

*L_i, C_i are the L_{hi}, C_{hi} ($n = o, e, \gamma$) symbols, referred to Z_{ev}, Z_{od} or Z_{γ}, respectively.

TABLE IV
BREAKDOWN OF THE EQUIVALENT CIRCUIT IN FIG. 10 FOR THE 0.353 × 0.051 cm STRUCTURE

	Residual Inductance
	L_R (nH)
$2Z_{\bar{ev}}$	0.0365
$2Z_{\bar{od}}$	0.1099
$2Z_{\gamma}$	0.0853

16 GHz. The equivalent length b_{eq} considered for the stubs is 0.193 cm and 0.243 cm, respectively.

RESULTS AND COMMENTS

The proposed modeling of double step discontinuities and the alternative approach for open stubs in shunt connection has been experimentally tested through microstrip rectangular structures realized on alumina substrate.

The simulation results, achieved by implementing the equivalent circuit of the double step discontinuity into a commercial CAD package (Touchstone®) are reported in Fig. 15(a) and (b) for the l = 0.68 cm and the l = 0.9 cm structures respectively (in both cases b = 1.5 cm). Those theoretical results are compared with the experi-

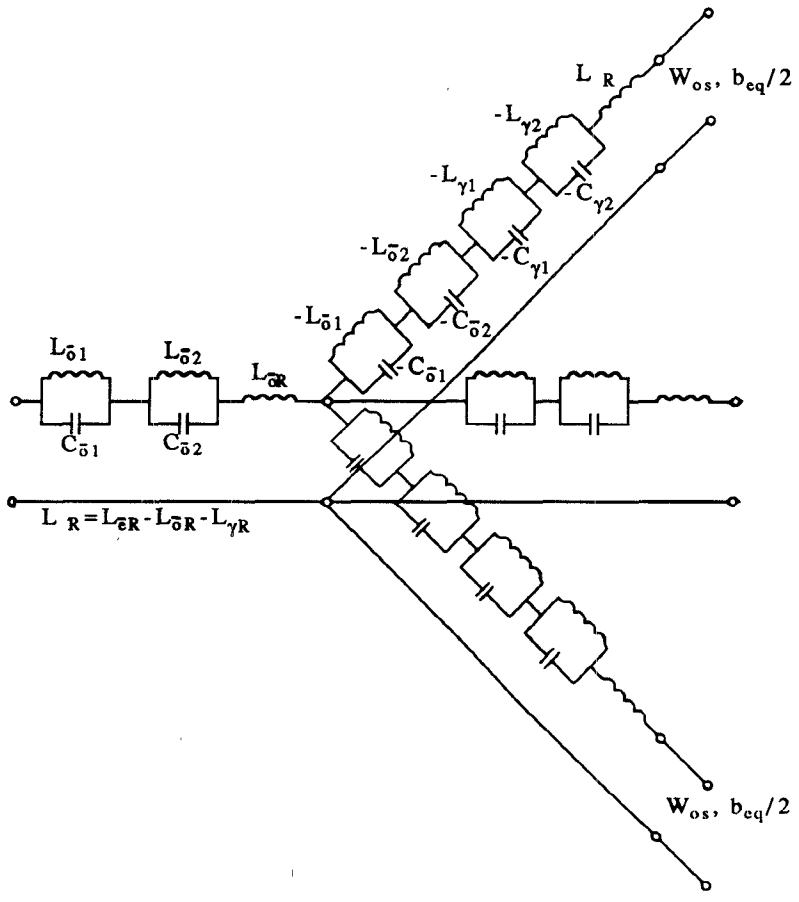

Fig. 11. Cross junction based equivalent circuit for the 1.5 × 0.68 cm rectangular microstrip structure.

TABLE V
BREAKDOWN OF THE EQUIVALENT CIRCUIT IN FIG. 11 FOR THE 1.5 × 0.68 cm STRUCTURE

	First Cell		Second Cell		Residual Inductance
	L_1 (nH)	C_1 (pF)	L_2 (nH)	C_2 (pF)	L_R (nH)
$2Z_{\tilde{ev}}$	—	—	—	—	0.2920
$2Z_{\tilde{od}}$	0.1466	3.5336	0.1553	1.7417	0.2674
$2Z_{\tilde{\gamma}}$	0.0064	84.3732	0.0059	13.7205	0.0230

ments carried out on the alumina samples (0.0635 cm thick substrate, with $\epsilon_r = 9.7$) and with the simulation data based on the Touchstone® "mstep" model (Fig. 15(a)).

The comparison between simulations and experiments has also been performed by adopting the alternative model for shunt-connected open stubs. The results are displayed in Figs. 16 (a,b,c) for the $b = 0.785$ cm × $l = 0.051$ cm structure, the 0.353 × 0.051 cm one (0.0254 cm thick substrate with $\epsilon_r = 9.9$) and the above $b = 1.5$ cm × $l = 0.68$ cm structure. In Fig. 16(c) the simulation results are also compared with those based on the Touchstone® "mcross" model.

A further comparison between theory and experiments is reported in Fig. 17(a) and (b) testing the tee junction based model for the $b = 0.176 \times l = 0.051$ cm structure

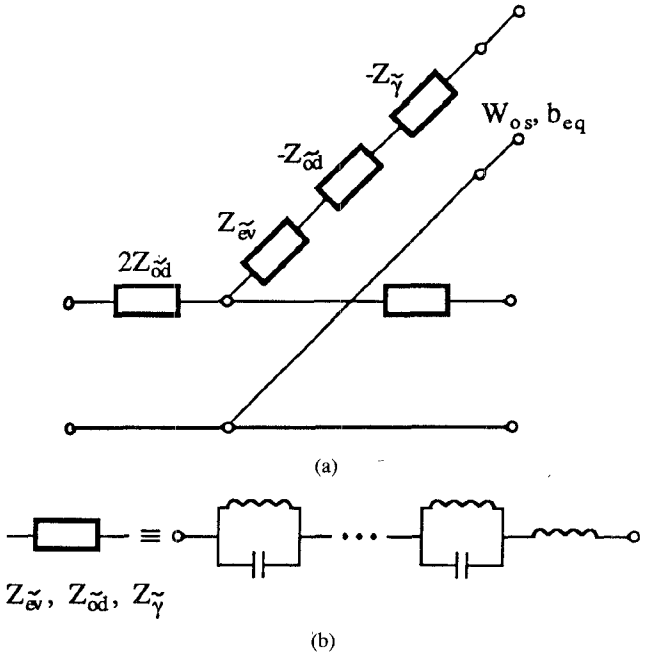

Fig. 12. (a) Tee junction based equivalent circuit for a rectangular microstrip structure. (b) Detail of the $Z_{ev}Z_{od}Z_{\tilde{\gamma}}$ block.

and the $b = 0.226 \times l = 0.051$ cm one (0.0254 cm thick substrate with $\epsilon_r = 9.9$).

The examples here reported show a good agreement with the experimental results in wide frequency ranges

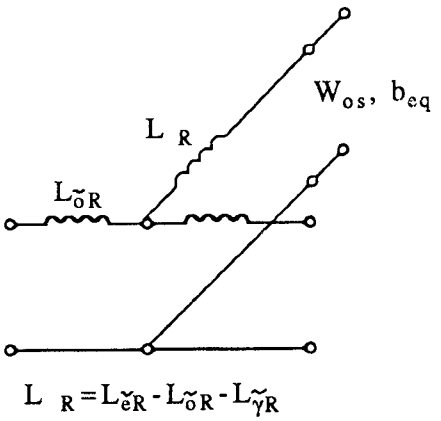

Fig. 13. Tee junction based equivalent circuit for a rectangular microstrip structure with $b = 0.176$ cm and $l = 0.051$ cm.

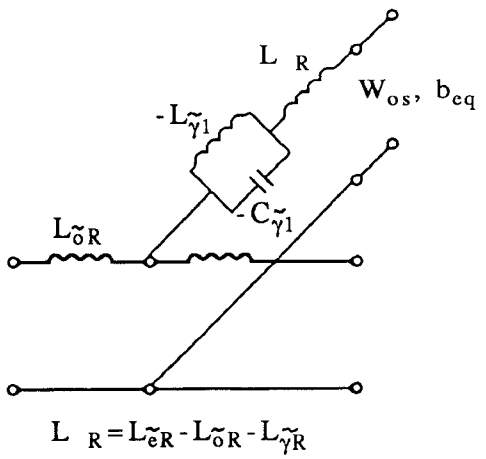

Fig. 14. Tee junction based equivalent circuit for a rectangular microstrip structure with $b = 0.226$ cm and $l = 0.051$ cm.

TABLE VI
BREAKDOWN OF THE EQUIVALENT CIRCUIT IN FIG. 13 FOR THE 0.176 × 0.051 cm STRUCTURE

	Residual Inductance L_R (nH)
Z_{ev}	0.0188
Z_{od}	0.0600
$Z_{\tilde{\gamma}}$	0.1083

TABLE VII
BREAKDOWN OF THE EQUIVALENT CIRCUIT IN FIG. 14 FOR THE 0.226 × 0.051 cm STRUCTURE

	First Cell		Residual Inductance
	L_1 (nH)	C_1 (pF)	L_R (nH)
Z_{ev}	—	—	0.0185
Z_{od}	—	—	0.0587
$Z_{\tilde{\gamma}}$	0.0194	2.4989	0.0829

and for various structure size. On the contrary, many models—in particular some of those included in commercial software as depicted in Figs. 15(a) and 16(c)—are

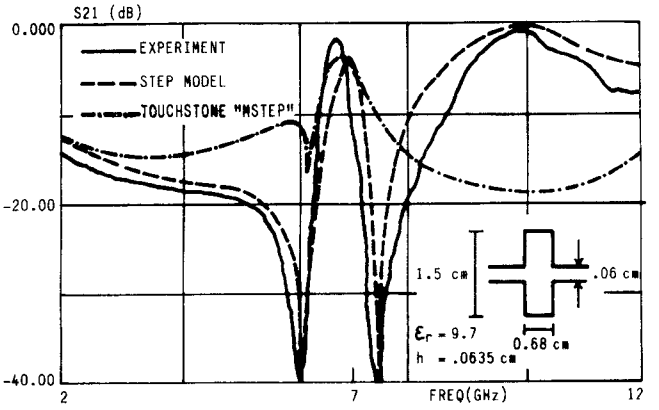

(a)

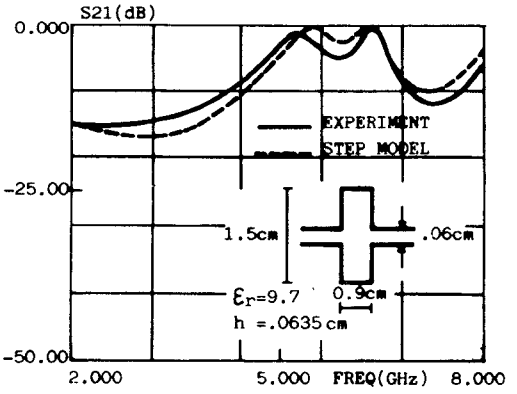

(b)

Fig. 15. Comparison between experiments and theoretical simulations via the step discontinuity model for: (a) 1.5 × 0.68 cm structure; (b) 1.5 × 0.9 cm structure.

acceptable in accuracy when the rectangular microstrip is narrow in width but become extremely poor for wide transversal dimensions especially in the higher frequency region [12].

The noticeable flexibility of the proposed approach derives from the equivalent circuit independence on the structure geometry. This implies that both the step-discontinuity and the cross-junction model can be adopted for a given structure, bringing to different equivalent circuits but to the same simulation results. This appears to be a particularly important feature, especially in a geometry-based optimization routines. It is well known, in fact, that the possible achievement of non-meaningful parameter values, due to an unadvised overcoming of the validity range of the used models, represents one of the limits of commercial CAD software packages.

The congruency of the simulations performed through the use of two different equivalent circuits corresponding to the same structure ($b = 1.5$ cm, $l = 0.68$ cm), considered as a double step discontinuity and as a double stub in shunt connection, is pointed out by comparing the theoretical results reported in Figs. 15(a) and 16(c).

In practical cases the structure geometrical ratio (l/b) may advise the use of either one of the two models, optimizing model effectiveness and simplicity. The step-dis-

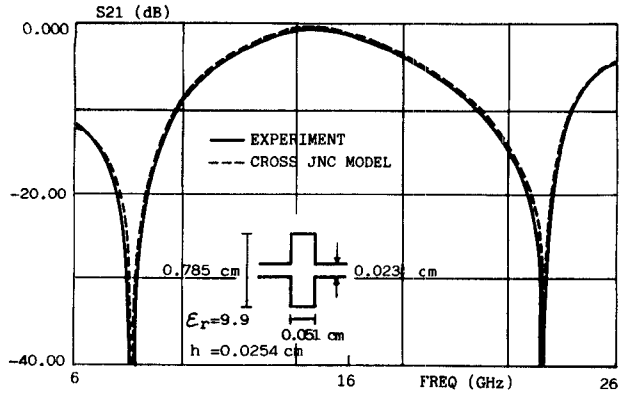

(a)

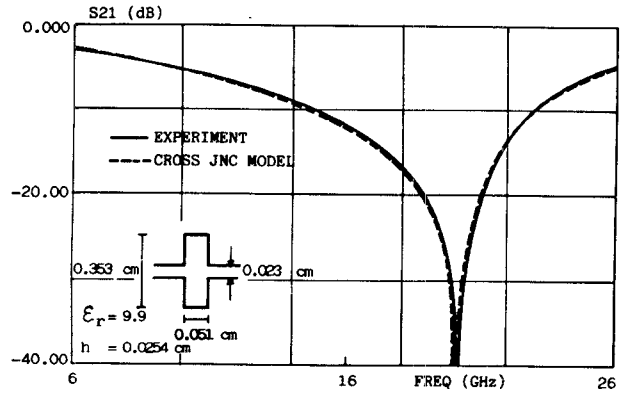

(b)

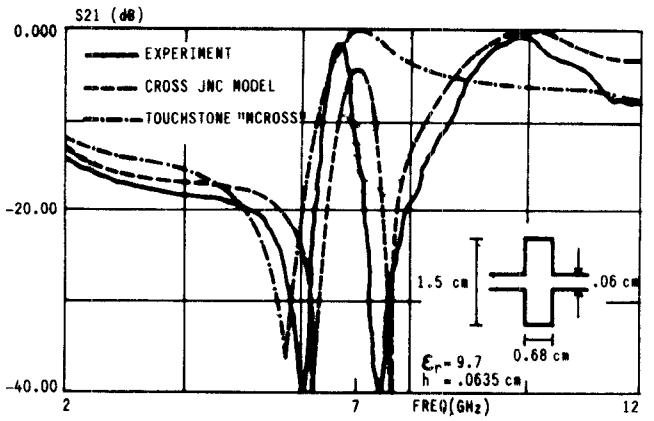

(c)

Fig. 16. Comparison between experiments and theoretical simulations via the cross junction based model for: (a) 0.785 × 0.051 cm and (b) 0.353 × 0.051 cm (experiments courtesy from EESOF); (c) 1.5 × 0.68 cm structures.

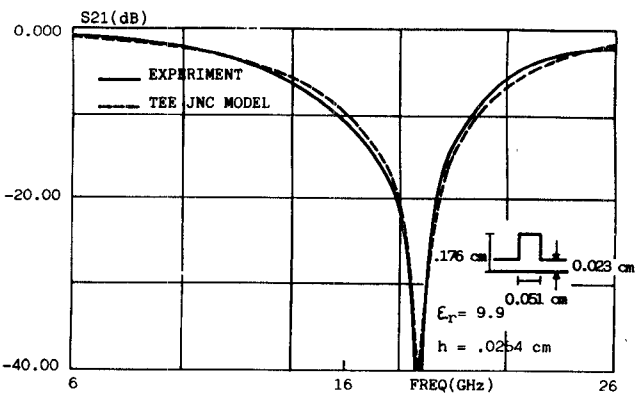

(a)

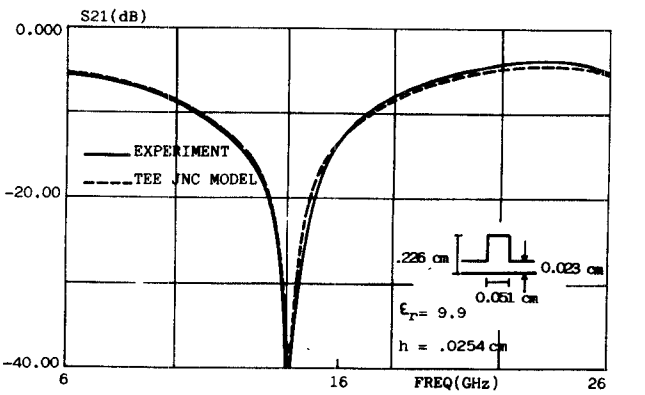

(b)

Fig. 17. Comparison between experiments (courtesy from EESOF) and theoretical simulations in the tee junction based model for: (a) 0.176 × 0.051 cm structure; (b) 0.226 × 0.051 cm structure.

continuity model could be more properly used when geometrical ratio l/b is lower than $1/2$.

An additional feature which arises from using the proposed models consists of a noticeable enhancement in the computational speed. In fact, while the modal analysis implementation normally requires the evaluation of several tens of modes at each frequency, the lumped element equivalent circuit is evaluated at only a single frequency, through the use of the same number of modes, and then swept in frequency to perform a broadband simulation. The computation time can be reduced by at least an order of magnitude, without a significant reduction of the achievable accuracy.

V. Conclusion

The newly developed modeling of the discontinuities introduced by a microstrip rectangular structure allows the overcoming of geometry and frequency limitations or poor accuracy of both past approaches and most of the presently available models.

A number of features characterize the proposed models, such as the simple and designer-oriented approach, the flexibility, the computational time saving.

The proposed further modelling for double shunt connected open stubs, which can be used as an alternative to the step discontinuity one to match different structure dimensions, always brings to the same results as the other one when simulating the same structure.

The approach can be utilized also for single shunt connected stubs.

Experiments fully confirm the effectiveness of the proposed modelling approach and propose it as useful tool in the design of microwave and millimeter-wave monolithic integrated circuits.

ACKNOWLEDGMENT

The authors wish to thank Dr. C. Holmes from EESOF Inc. for providing some of the experimental data and Prof. V. K. Tripathi for helpful discussion and suggestions.

REFERENCES

[1] C. J. Railton and T. Rozzi, "The rigorous analysis of cascaded step discontinuities in microstrip," *IEEE Trans. Microwave Theory Tech.*, vol. 36, no. 7, pp. 1177–1185, July 1988.

[2] N. Koster and R. H. Jansen, "The microstrip discontinuity—A revised description," *IEEE Trans. Microwave Theory Tech.*, vol. 34, no. 2, pp. 213–223, Feb. 1986.

[3] W. Menzel and I. Wolff, "A method for calculating the frequency dependent properties of microstrip discontinuities," *IEEE Trans. Microwave Theory Tech.*, vol. 25, no. 2, pp. 107–112, Feb. 1977.

[4] T. K. Chu, T. Itoh, and Y. Shih, "Comparative study of mode-matching formulations for microstrip discontinuity problems," *IEEE Trans. Microwave Theory Tech.*, vol. 33, no. 10, pp. 1018–1023, Oct. 1985.

[5] G. Kompa, "S-matrix comparation of microstrip discontinuities with a planar waveguide model," *AEU*, vol. 30, pp. 58–64, 1976.

[6] ——, "Design of stepped microstrip components," *Radio Electron. Eng.*, pp. 53–63, Jan.–Feb. 1978.

[7] G. D'Inzeo, F. Giannini, and R. Sorrentino, "Wide-band equivalent circuit of microwave planar networks," *IEEE Trans. Microwave Theory Tech.*, vol. 28, no. 10, pp. 1107–1113, Oct. 1980.

[8] F. Giannini, G. Bartolucci, and M. Ruggieri, "Enhanced model for interacting step-discontinuities," in *IEEE MTT-S Int. Microwave Symp. Dig.*, vol. I-G6, pp. 251–254, Long Beach, CA, June 1989.

[9] B. Bianco, M. Granara, and S. Ridella, "Filtering properties of two-dimensional lines discontinuities," *Alta Frequenza*, vol. XLII, pp. 140E–148E, July 1973.

[10] F. Giannini, G. Bartolucci, and M. Ruggieri, "An improved equivalent model for microstrip cross-junction," in *Proc. 19th European Microwave Conf.*, London, Sept. 1989, pp. 1226–1231.

[11] G. D'Inzeo, F. Giannini, C. M. Sodi, and R. Sorrentino, "Method of analysis and filtering properties of microwave planar networks," *IEEE Trans. Microwave Theory Tech.*, vol. 26, no. 7, pp. 462–471, July 1978.

[12] F. Giannini, G. Bartolucci, M. Ruggieri, "Low-impedance matching: the straight stub solution," *Microwave and Optical Technology Lett.*, vol. 2, no. 3, pp. 96–101, Mar. 1989.

[13] I. Wolff and N. Knoppik, "Rectangular and circular microstrip disk capacitors, and resonators," *IEEE Trans. Microwave Theory Tech.*, vol. MTT-22, no. 10, pp. 857–864, Oct. 1974.

[14] F. Giannini, M. Salerno, and R. Sorrentino: "Effects of parasitics in lowpass elliptic filters for MIC," *Electron Lett.*, vol. 13, no. 7, pp. 284–285, Apr. 1988.

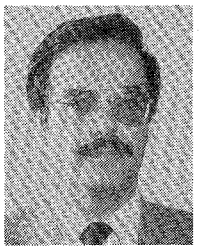

Franco Giannini was born in Galatina, Italy, in 1944. He received his degree in Electronics Engineering from the University of Rome 'La Sapienza' in 1968.

In 1968 he joined the Institute of Electronics of "La Sapienza," where he was Assistant Professor until 1980. He was also Associate Professor of Microwaves at the University of Ancona, Italy (1973–1974), and of both Solid-State Electronics (1974–1977) and Applied Electronics (1977–1980) at the University of Rome "La Sapienza." In 1980 he became Full Professor of Applied Electronics at "La Sapienza."

Since 1981 he has been with the II University of Rome "Tor Vergata." He has been working on problems concerning theory of active and passive microwave components, including GaAs monolithic circuits. He is currently chairing the theme "Monolithic integrated circuits in the 20–30 GHz bandwidth" of the CNR's National Project "Solid State Electronic Devices." He is author and co-author of more than 100 technical papers. Mr. Giannini is a consultant for various national and international industrial and governmental organizations.

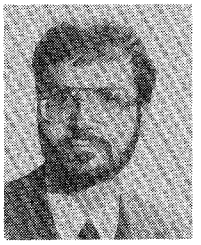

Giancarlo Bartolucci was born in Rome in 1958. He graduated cum laude in 1982 in Electronics Engineering from the University of Rome "La Sapienza," with a thesis on integrated optics.

In 1982 he was with Fondazione U. Bordoni, Rome, Italy. In 1983 he served as an Officer in the Technical Corps of the Army. Since 1984 he has been a Research and Teaching Assistant with the Department of Electronics Engineering at the II University of Rome "Tor Vergata." His current research interests are in the field of propagation in microwave and millimeter wave transmission lines in the field of active antennas for satellite applications.

Marina Ruggieri (S'84–M'85) was born in Napoli, Italy in 1961. She received the electronics engineering degree in 1984 from the University of Rome "La Sapienza." Her thesis dealt with the 12 GHz DBS receiver and it was carried out during a stage period at FACE (ITT) Research Center, Pomezia, Italy.

In 1985 she was with FACE (ITT) in the High Frequency Division and sent to the Gallium Arsenide Technology Center (GTC-ITT, Roanoke, VA) for a period of training on GaAs monolithic design and fabrication techniques. She was with FACE (ITT) up to 1986. From June 1986 to October 1991, she was a Research and Teaching Assistant at the Department of Electronics Engineering of the II University of Rome "Tor Vergata." Since November 1991, she has been Associate Professor of "Signal Theory" at the Department of Electrical Engineering of the University of L'Aquila. Her research mainly concerns feasibility study, characterization and design of radio systems for fixed and mobile communications.